On the Reduction of Numerical Dissipation in Central-Upwind Schemes

Alexander Kurganov[1,*] and Chi-Tien Lin[2]

[1] *Department of Mathematics, Tulane University, New Orleans, LA 70118, USA/ Department of Mathematics, University of Michigan, Ann Arbor, MI 48109, USA.*

[2] *Department of Applied Mathematics, Providence University, Shalu, 433, Taiwan.*

Abstract. We study central-upwind schemes for systems of hyperbolic conservation laws, recently introduced in [13]. Similarly to staggered non-oscillatory central schemes, these schemes are central Godunov-type projection-evolution methods that enjoy the advantages of high resolution, simplicity, universality and robustness. At the same time, the central-upwind framework allows one to decrease a relatively large amount of numerical dissipation present at the staggered central schemes. In this paper, we present a modification of the one-dimensional fully- and semi-discrete central-upwind schemes, in which the numerical dissipation is reduced even further. The goal is achieved by a more accurate projection of the evolved quantities onto the original grid. In the semi-discrete case, the reduction of dissipation procedure leads to a new, less dissipative numerical flux. We also extend the new semi-discrete scheme to the two-dimensional case via the rigorous, genuinely multidimensional derivation. The new semi-discrete schemes are tested on a number of numerical examples, where one can observe an improved resolution, especially of the contact waves.

AMS subject classfications: 65M10, 65M12, 35L65

Key words: Hyperbolic systems of conservation laws, Godunov-type finite-volume methods, central-upwind schemes, numerical dissipation.

1 Introduction

Consider the systems of hyperbolic conservation laws:

$$\frac{\partial}{\partial t}\mathbf{u}(\mathbf{x},t) + \nabla_{\mathbf{x}} \cdot \mathbf{f}(\mathbf{u}(\mathbf{x},t)) = \mathbf{0}, \tag{1.1}$$

*Corresponding author. *Email addresses:* kurganov@math.tulane.edu (A. Kurganov), ctlin@pu.edu.tw (C. T. Lin)

where $\mathbf{u}(\mathbf{x},t) = (u_1(\mathbf{x},t),...,u_N(\mathbf{x},t))^T$ is an N-dimensional vector and $\mathbf{f}$ is a nonlinear convection flux. In the general multidimensional case, $\mathbf{u}$ is a vector function of a time variable t and d-spatial variables $\mathbf{x} = (x_1,...,x_d)$ with the corresponding fluxes $\mathbf{f} = (f^1,...,f^d)$. Such systems arise in many different applications, for instance, in fluid mechanics, geophysics, meteorology, astrophysics, financial and biological modeling, multi-component flows, groundwater flow, semiconductors, reactive flows, geometric optics, traffic flow, and other areas.

We study numerical methods for system (1.1). In particular, we are interested in Godunov-type finite-volume central schemes, which are *simple, robust* and *universal* Riemann-problem-solver-free methods for general systems of conservation laws. The key idea in their construction is the integration over the control volumes that contain the entire Riemann fans. Such a setting allows one to evolve a piecewise polynomial projections of the computed solution to the next time level without (approximately) solving (generalized) Riemann problems, arising at cell interfaces.

The prototype central scheme is the celebrated (staggered) Lax-Friedrichs scheme [3, 19]. This is a very dissipative first-order scheme, which typically cannot provide a satisfactory resolution of discontinuities and rarefaction corners unless a very large number of grid points is used. Its higher-order (and also higher resolution) generalization was proposed by Nessyahu and Tadmor in [28]. Later the one-dimensional (1-D) second-order Nessyahu-Tadmor scheme was extended to higher orders [22, 26] and to more than one spatial dimensions [1, 7, 24]. Its nonstaggered version was proposed in [6].

The major drawback of staggered central schemes is their relatively large numerical dissipation. This makes them inappropriate for large time integrations, steady-state computations, and for the cases where small time steps are enforced, for example, due to the presence of source or diffusion terms on the right-hand side (RHS) of (1.1). They also do not admit a semi-discrete form, which may be particularly advantageous in the latter case (see, e.g., [8, 10, 12, 17]).

In order to eliminate the aforementioned disadvantages, a new class of high-resolution central schemes has been recently proposed in [17]. The main idea in the construction of the new central schemes is to utilize the *local propagation speeds* to obtain a more precise estimate on the width of Riemann fans. The solution is then evolved separately in "non-smooth" (those that include Riemann fans) and "smooth" control volumes, and the resulting nonuniformly distributed data are projected back onto the original, *non-staggered* grid. The higher-order extensions of this scheme were proposed in [11, 14, 18], and its genuinely multidimensional generalization was obtained in [14].

The numerical dissipation present at central schemes can be further reduced by utilizing *one-sided* local propagation speeds. This leads to the so-called *central-upwind schemes*, recently introduced in [13]. This class of schemes enjoys all the major advantages of Riemann-problem-solver-free central schemes — high efficiency, simplicity and universality. At the same time, it has a certain upwind nature (more information on the directions of wave propagation is utilized since the control volumes over the Riemann fans are no longer symmetric), which leads to a higher resolution.

In this paper, we implement an idea of less dissipative projection step, suggested in the context of partial characteristic decomposition in [15]. This leads to new 1-D fully- and semi-discrete central-upwind schemes with even smaller numerical viscosity and, as a result, to a further improvement in the resolution of nonsmooth parts of the solution, especially of contact waves. Finally, this approach is generalized for two-dimensional (2-D) systems, and a new multidimensional semi-discrete central-upwind scheme is introduced.

The paper is organized as follows. In Section 2, we derive our new fully-discrete scheme, which is reduced to a simpler semi-discrete version in Section 3. A new 2-D semi-discrete central-upwind scheme is then constructed in Section 4. Finally, the new schemes are tested on a number of 1-D and 2-D examples in Section 5.

2 One-dimensional fully-discrete scheme

In this section, we describe the construction of the new second-order fully-discrete central-upwind scheme for the 1-D system of hyperbolic conservation laws:

$$\mathbf{u}_t + \mathbf{f}(\mathbf{u})_x = \mathbf{0}. \tag{2.1}$$

The scheme is based on the integral form of the system of conservation laws obtained by integrating (2.1) over control volumes and consists of three consecutive steps — *reconstruction*, *evolution* and *projection*.

For simplicity, we only consider uniform grids: $x_\alpha := \alpha \Delta x$, $t^\beta := \beta \Delta t$, $\lambda := \Delta t / \Delta x$. We also assume that at a certain time level $t = t^n$ the computed *cell averages* of the solution:

$$\bar{\mathbf{u}}_j^n \approx \frac{1}{\Delta x} \int\limits_{x_{j-\frac{1}{2}}}^{x_{j+\frac{1}{2}}} \mathbf{u}(x,t^n)\,dx,$$

are available. Then, the evolution of the computed solution to the next time level $t = t^{n+1}$ can be presented as follows.

Step 1: Reconstruction

First, using the cell averages $\{\bar{\mathbf{u}}_j^n\}$ we reconstruct a second-order piecewise linear interpolant:

$$\widetilde{\mathbf{u}}(x,t^n) = \sum_j [\bar{\mathbf{u}}_j^n + \mathbf{s}_j^n (x - x_j)] \chi_j(x). \tag{2.2}$$

Here, $\mathbf{s}_j^n$ are slopes of the corresponding linear pieces and $\chi_j(x)$ is the characteristic function over the cell $(x_{j-1/2}, x_{j+1/2})$. Such an interpolant will be second-order accurate provided the slopes $\mathbf{s}_j^n$ are (at least) first-order approximations of the spatial derivatives

$\mathbf{u}_x(x_j, t^n)$. To avoid oscillations that may appear at cell interfaces $\{x_{j+1/2}\}$, a *nonlinear limiter* should be used in the evaluation of the slopes. We will use the generalized minmod limiter (see, e.g., [20, 25, 28, 29]):

$$\mathbf{s}_j^n = \text{minmod}\left(\theta\frac{\bar{\mathbf{u}}_{j+1}^n - \bar{\mathbf{u}}_j^n}{\Delta x}, \frac{\bar{\mathbf{u}}_{j+1}^n - \bar{\mathbf{u}}_{j-1}^n}{2\Delta x}, \theta\frac{\bar{\mathbf{u}}_j^n - \bar{\mathbf{u}}_{j-1}^n}{\Delta x}\right), \quad \theta \in [1,2], \tag{2.3}$$

where the minmod function is defined as follows:

$$\text{minmod}(c_1, c_2, \ldots, c_m) := \begin{cases} \min(c_1, c_2, \ldots, c_m), & \text{if } c_i > 0 \ \forall i = 1, \ldots, m, \\ \max(c_1, c_2, \ldots, c_m), & \text{if } c_i < 0 \ \forall i = 1, \ldots, m, \\ 0, & \text{otherwise.} \end{cases}$$

Note that larger values of θ correspond to sharper, more compressive, but also more oscillatory reconstructions (see, e.g., [25, 28]).

For the description of other nonlinear limiters that can be also used in the reconstruction step, we refer the reader to [5, 20, 21, 25, 28, 29] and the reference therein.

Step 2: Evolution

We begin with noting that due to the hyperbolicity of (2.1), the discontinuities appearing at the reconstruction step at the interface points $\{x_{j+1/2}\}$ propagate at finite speeds. Upper bounds on the right- and left-sided local speeds can be computed by

$$a_{j+\frac{1}{2}}^+ := \max_{\boldsymbol{\omega} \in C(\mathbf{u}_{j+\frac{1}{2}}^-, \mathbf{u}_{j+\frac{1}{2}}^+)} \left\{\lambda_N(A(\boldsymbol{\omega})), 0\right\}, \qquad a_{j+\frac{1}{2}}^- := \min_{\boldsymbol{\omega} \in C(\mathbf{u}_{j+\frac{1}{2}}^-, \mathbf{u}_{j+\frac{1}{2}}^+)} \left\{\lambda_1(A(\boldsymbol{\omega})), 0\right\}, \tag{2.4}$$

respectively. Here, $\lambda_1 < \lambda_2 < \ldots < \lambda_N$ are the N eigenvalues of the Jacobian $A := \partial\mathbf{f}/\partial\mathbf{u}$, and $C(\mathbf{u}_{j+1/2}^-, \mathbf{u}_{j+1/2}^+)$ is the Riemann admissible curve in the phase space that connects the left, $\mathbf{u}_{j+1/2}^-$, and the right, $\mathbf{u}_{j+1/2}^+$, states:

$$\mathbf{u}_{j+\frac{1}{2}}^- := \lim_{x \to x_{j+\frac{1}{2}}^-} \widetilde{\mathbf{u}}(x, t^n) = \bar{\mathbf{u}}_j^n + \frac{\Delta x}{2}\mathbf{s}_j^n, \quad \mathbf{u}_{j+\frac{1}{2}}^+ := \lim_{x \to x_{j+\frac{1}{2}}^+} \widetilde{\mathbf{u}}(x, t^n) = \bar{\mathbf{u}}_{j+1}^n - \frac{\Delta x}{2}\mathbf{s}_{j+1}^n. \tag{2.5}$$

In the case of convex flux $\mathbf{f}$, the local speeds can be estimated as follows:

$$a_{j+\frac{1}{2}}^+ := \max\left\{\lambda_N(A(\mathbf{u}_{j+\frac{1}{2}}^-)), \lambda_N(A(\mathbf{u}_{j+\frac{1}{2}}^+)), 0\right\},$$

$$a_{j+\frac{1}{2}}^- := \min\left\{\lambda_1(A(\mathbf{u}_{j+\frac{1}{2}}^-)), \lambda_1(A(\mathbf{u}_{j+\frac{1}{2}}^+)), 0\right\}.$$

It is more complicated to estimate the local speeds in the nonconvex case, we refer the reader to [16, 31], devoted to Godunov-type schemes for hyperbolic (systems of) conservation laws with nonconvex fluxes.
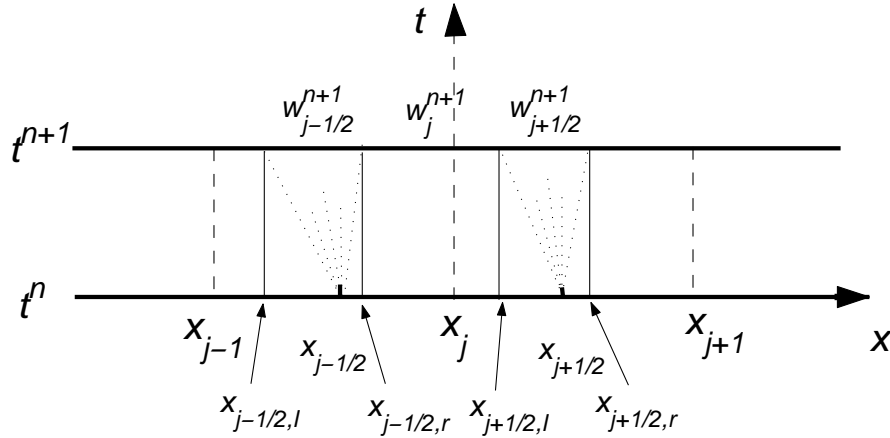
Figure 1: Control volumes selected according to nonsmooth and smooth areas.

Next, we split the strip $S = X \times [t^n, t^{n+1}]$, where X is a spatial computational domain, into the *nonsmooth*, $[x_{j+1/2,l}, x_{j+1/2,r}] \times [t^n, t^{n+1}]$, and *smooth*, $[x_{j-1/2,r}, x_{j+1/2,l}] \times [t^n, t^{n+1}]$, areas. Here,

$$x_{j+\frac{1}{2},l} := x_{j+\frac{1}{2}} + a_{j+\frac{1}{2}}^{-} \Delta t, \qquad x_{j+\frac{1}{2},r} := x_{j+\frac{1}{2}} + a_{j+\frac{1}{2}}^{+} \Delta t,$$

see Fig. 1. Obviously, such a partition of S is possible only provided the following CFL condition is satisfied:

$$\Delta t \cdot \max_{j} \left\{ \max \left(a_{j+\frac{1}{2}}^{+}, -a_{j+\frac{1}{2}}^{-} \right) \right\} < \frac{\Delta x}{2}.$$

Finally, we evolve the solution from time level $t = t^n$ to t^{n+1} by integrating (2.1) over the aforementioned smooth and nonsmooth areas, selected to be the control volumes. Using the midpoint quadrature for the temporal integrals, we obtain the following (intermediate) cell averages at time $t = t^{n+1}$, over the nonsmooth areas:

$$\bar{\mathbf{w}}_{j+\frac{1}{2}}^{n+1} = \frac{1}{a_{j+\frac{1}{2}}^{+} - a_{j+\frac{1}{2}}^{-}} \left\{ \mathbf{u}_{j+\frac{1}{2},r}^{n} a_{j+\frac{1}{2}}^{+} - \frac{\mathbf{s}_{j+1}^{n}}{2} (a_{j+\frac{1}{2}}^{+})^2 \Delta t - \mathbf{u}_{j+\frac{1}{2},l}^{n} a_{j+\frac{1}{2}}^{-} + \frac{\mathbf{s}_{j}^{n}}{2} (a_{j+\frac{1}{2}}^{-})^2 \Delta t \right.$$
$$\left. - \left[\mathbf{f}(\mathbf{u}_{j+\frac{1}{2},r}^{n+\frac{1}{2}}) - \mathbf{f}(\mathbf{u}_{j+\frac{1}{2},l}^{n+\frac{1}{2}}) \right] \right\}, \tag{2.6}$$

and, similarly, over the smooth areas:

$$\bar{\mathbf{w}}_{j}^{n+1} = \bar{\mathbf{u}}_{j}^{n} + \frac{\mathbf{s}_{j}^{n}}{2} (a_{j+\frac{1}{2}}^{+} + a_{j+\frac{1}{2}}^{-}) \Delta t - \frac{\Delta t}{\Delta x - (a_{j-\frac{1}{2}}^{+} - a_{j+\frac{1}{2}}^{-}) \Delta t} \left[\mathbf{f}(\mathbf{u}_{j+\frac{1}{2},l}^{n+\frac{1}{2}}) - \mathbf{f}(\mathbf{u}_{j-\frac{1}{2},r}^{n+\frac{1}{2}}) \right]. \tag{2.7}$$

Here, the values of the piecewise linear reconstruction $\widetilde{\mathbf{u}}$ at $(x_{j+1/2,l}, t^n)$ and $(x_{j+1/2,r}, t^n)$ are:

$$\mathbf{u}_{j+\frac{1}{2},l}^{n} := \bar{\mathbf{u}}_{j}^{n} + \mathbf{s}_{j}^{n} \left(\frac{\Delta x}{2} + a_{j+\frac{1}{2}}^{-} \Delta t \right), \qquad \mathbf{u}_{j+\frac{1}{2},r}^{n} := \bar{\mathbf{u}}_{j+1}^{n} - \mathbf{s}_{j+1}^{n} \left(\frac{\Delta x}{2} - a_{j+\frac{1}{2}}^{+} \Delta t \right),$$

and the midpoint values, $\mathbf{u}_{j+1/2,l}^{n+1/2} \approx \mathbf{u}(x_{j+1/2,l}, t^{n+1/2})$ and $\mathbf{u}_{j+1/2,r}^{n+1/2} \approx \mathbf{u}(x_{j+1/2,r}, t^{n+1/2})$, can be obtained using the Taylor expansions about the corresponding points, $(x_{j+1/2,l}, t^n)$ and $(x_{j+1/2,r}, t^n)$:

$$\mathbf{u}_{j+\frac{1}{2},l}^{n+\frac{1}{2}} = \mathbf{u}_{j+\frac{1}{2},l}^n - \frac{\Delta t}{2} \mathbf{f}\left(\mathbf{u}_{j+\frac{1}{2},l}^n\right)_x, \qquad \mathbf{u}_{j+\frac{1}{2},r}^{n+\frac{1}{2}} = \mathbf{u}_{j+\frac{1}{2},r}^n - \frac{\Delta t}{2} \mathbf{f}\left(\mathbf{u}_{j+\frac{1}{2},r}^n\right)_x. \tag{2.8}$$

Note that one can avoid the computation of the Jacobians in (2.8) by using a component-wise evaluation of $\mathbf{f}_x$, consult [17, 28] for details.

Remark 2.1. The first two steps in the construction of the new central-upwind scheme are identical to the corresponding steps in [13, 15]. The novel feature of our scheme is in the next, projection step.

Step 3: Projection

At the final step, a piecewise linear interpolant,

$$\widetilde{\mathbf{w}}(x, t^{n+1}) \tag{2.9}$$
$$:= \sum_j \left\{ \left[\bar{\mathbf{w}}_{j+\frac{1}{2}}^{n+1} + \mathbf{s}_{j+\frac{1}{2}}^{n+1}\left(x - \frac{x_{j+\frac{1}{2},l} + x_{j+\frac{1}{2},r}}{2} \right) \right] \chi_{[x_{j+\frac{1}{2},l}, x_{j+\frac{1}{2},r}]} + \bar{\mathbf{w}}_j^{n+1} \chi_{[x_{j-\frac{1}{2},r}, x_{j+\frac{1}{2},l}]} \right\},$$

reconstructed from the evolved intermediate cell averages $\{\bar{\mathbf{w}}_j^{n+1}\}$ and $\{\bar{\mathbf{w}}_{j+1/2}^{n+1}\}$, is projected back onto the original grid by averaging it over the intervals $[x_{j-1/2}, x_{j+1/2}]$. This results in the new projected cell averages:

$$\bar{\mathbf{u}}_j^{n+1} = \lambda a_{j-\frac{1}{2}}^+ \bar{\mathbf{w}}_{j-\frac{1}{2}}^{n+1} + \left[1 + \lambda(a_{j-\frac{1}{2}}^- - a_{j+\frac{1}{2}}^+) \right] \bar{\mathbf{w}}_j^{n+1} - \lambda a_{j+\frac{1}{2}}^- \bar{\mathbf{w}}_{j+\frac{1}{2}}^{n+1}$$
$$+ \frac{\lambda \Delta t}{2} \left[\mathbf{s}_{j+\frac{1}{2}}^{n+1} a_{j+\frac{1}{2}}^+ a_{j+\frac{1}{2}}^- - \mathbf{s}_{j-\frac{1}{2}}^{n+1} a_{j-\frac{1}{2}}^+ a_{j-\frac{1}{2}}^- \right]. \tag{2.10}$$

In order to use this formula, the slopes $\{\mathbf{s}_{j+1/2}^{n+1}\}$ are to be evaluated. This can be done in several different ways. For instance, in [13,17], the most straightforward component-wise approach was implemented, namely, the slopes were computed by:

$$\mathbf{s}_{j+\frac{1}{2}}^{n+1} = 2 \cdot \text{minmod}\left(\theta \frac{\bar{\mathbf{w}}_{j+\frac{1}{2}}^{n+1} - \bar{\mathbf{w}}_j^{n+1}}{x_{j+\frac{1}{2},r} - x_{j-\frac{1}{2},r}}, \frac{\bar{\mathbf{w}}_{j+1}^{n+1} - \bar{\mathbf{w}}_j^{n+1}}{x_{j+\frac{3}{2},l} + x_{j+\frac{1}{2},r} - x_{j+\frac{1}{2},l} - x_{j-\frac{1}{2},r}}, \theta \frac{\bar{\mathbf{w}}_{j+1}^{n+1} - \bar{\mathbf{w}}_{j+\frac{1}{2}}^{n+1}}{x_{j+\frac{3}{2},l} - x_{j+\frac{1}{2},l}} \right),$$

see Fig. 2(a). Here, the distances

$$x_{j+\frac{1}{2},r} - x_{j-\frac{1}{2},r} = \Delta x + \Delta t(a_{j+\frac{1}{2}}^+ - a_{j-\frac{1}{2}}^+) \quad \text{and} \quad x_{j+\frac{3}{2},l} - x_{j+\frac{1}{2},l} = \Delta x + \Delta t(a_{j+\frac{3}{2}}^- - a_{j+\frac{1}{2}}^-)$$

are of order Δx for small Δt, and thus the slopes $\mathbf{s}_{j+1/2}^{n+1}$ are proportional to $\Delta \mathbf{w}/\Delta x$ as $\Delta t \sim 0$, which may lead to a scheme with a relatively large numerical dissipation. This can be
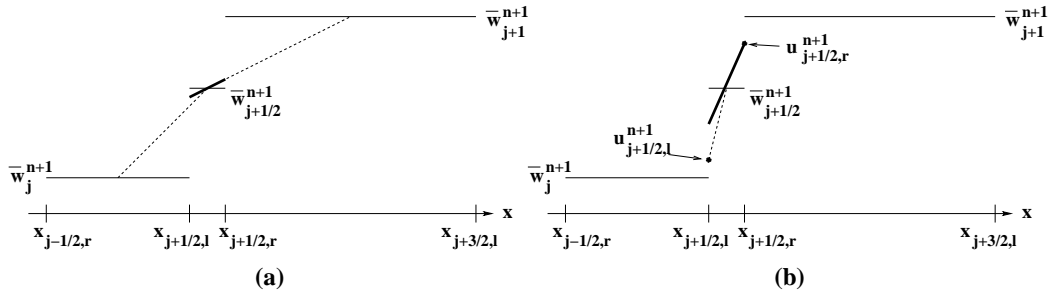
Figure 2: Computing the slope $s_{j+1/2}^{n+1}$: (a) the approach from [13, 17] vs. (b) the new, less dissipative approach.

understood if one looks at the last term on the RHS of (2.10). If we assume that Δx is fixed, then this term is of order $(\Delta t)^2$, and hence when the time-steps are small, the contribution of the nonzero slopes in the linear reconstruction (2.9) may become negligible, which would make the projection step to be as diffusive as a first-order projection typically is.

In this paper, we propose an alternative, less dissipative way of computing $\mathbf{s}_{j+1/2}^{n+1}$. First, we approximate the values of the solution at the points $x_{j+1/2,l}$ and $x_{j+1/2,r}$ at the new time level $t = t^{n+1}$, which will be denoted by $\mathbf{u}_{j+1/2,l}^{n+1}$ and $\mathbf{u}_{j+1/2,r}^{n+1}$, respectively. Since the solution of the initial-value problem (2.1)–(2.2) is smooth there, we may use the corresponding Taylor expansions, which, similarly to (2.8), give:

$$\mathbf{u}_{j+\frac{1}{2},l}^{n+1} = \mathbf{u}_{j+\frac{1}{2},l}^{n} - \Delta t \mathbf{f}\left(\mathbf{u}_{j+\frac{1}{2},l}^{n}\right)_x, \qquad \mathbf{u}_{j+\frac{1}{2},r}^{n+1} = \mathbf{u}_{j+\frac{1}{2},r}^{n} - \Delta t \mathbf{f}\left(\mathbf{u}_{j+\frac{1}{2},r}^{n}\right)_x. \qquad (2.11)$$

To prevent the reconstruction (2.9) from being oscillatory, we need to enforce the monotonicity of these values. Namely, if $\mathbf{u}_{j+1/2,l}^{n+1}$ ($\mathbf{u}_{j+1/2,r}^{n+1}$), computed in (2.11), is not between $\bar{\mathbf{w}}_j^{n+1}$ and $\bar{\mathbf{w}}_{j+1}^{n+1}$, we set $\mathbf{u}_{j+1/2,l}^{n+1} := \bar{\mathbf{w}}_j^{n+1}$ ($\mathbf{u}_{j+1/2,r}^{n+1} := \bar{\mathbf{w}}_{j+1}^{n+1}$).

We then apply the minmod limiter to these point values and to the cell average $\bar{\mathbf{w}}_{j+1/2}^{n+1}$, which is, due to the conservativeness of the reconstruction (2.9), equal to the point value at the center of the nonsmooth area $[x_{j+1/2,l}, x_{j+1/2,r}]$. This results in:

$$\mathbf{s}_{j+\frac{1}{2}}^{n+1} = \text{minmod}\left(\frac{\bar{\mathbf{w}}_{j+\frac{1}{2}}^{n+1} - \mathbf{u}_{j+\frac{1}{2},l}^{n+1}}{\delta}, \frac{\mathbf{u}_{j+\frac{1}{2},r}^{n+1} - \bar{\mathbf{w}}_{j+\frac{1}{2}}^{n+1}}{\delta}\right), \qquad (2.12)$$

where $\delta := \frac{\Delta t}{2}(a_{j+1/2}^+ - a_{j+1/2}^-)$ is equal to the length of the interval $[x_{j+1/2,l}, x_{j+1/2,r}]$.

This completes the construction of the new 1-D second-order fully-discrete central-upwind scheme (2.10) with (2.3)–(2.8) and (2.11)–(2.12).

Remark 2.2. The advantage of the new projection — reduced numerical dissipation — is further amplified when one passes to a semi-discrete limit as $\Delta t \rightarrow 0$, because unlike the case, studied in [13], the last term on the RHS of (2.10) will have a nonzero contribution to the semi-discrete numerical flux. The derivation of the new semi-discrete central-upwind scheme is presented in the next section.

3   One-dimensional semi-discrete scheme

In this section, we reduce the fully-discrete scheme, derived in Section 2, to its much simpler, semi-discrete version.

We proceed along the lines of [13, 15, 17]. First, from (2.10) we obtain:

$$
\begin{aligned}
\frac{d}{dt}\bar{\mathbf{u}}_j(t^n) &= \lim_{\Delta t \to 0} \frac{\bar{\mathbf{u}}_j^{n+1} - \bar{\mathbf{u}}_j^n}{\Delta t} \\
&= \frac{a_{j-\frac{1}{2}}^+}{\Delta x} \lim_{\Delta t \to 0} \bar{\mathbf{w}}_{j-\frac{1}{2}}^{n+1} + \lim_{\Delta t \to 0} \left\{ \frac{\left[1 + \lambda(a_{j-\frac{1}{2}}^- - a_{j+\frac{1}{2}}^+) \right] \bar{\mathbf{w}}_j^{n+1} - \bar{\mathbf{u}}_j^n}{\Delta t} \right\} \\
&\quad - \frac{a_{j+\frac{1}{2}}^-}{\Delta x} \lim_{\Delta t \to 0} \bar{\mathbf{w}}_{j+\frac{1}{2}}^{n+1} + \frac{1}{2\Delta x} \lim_{\Delta t \to 0} \left[\Delta t \left(\mathbf{s}_{j+\frac{1}{2}}^{n+1} a_{j+\frac{1}{2}}^+ a_{j+\frac{1}{2}}^- - \mathbf{s}_{j-\frac{1}{2}}^{n+1} a_{j-\frac{1}{2}}^+ a_{j-\frac{1}{2}}^- \right) \right].
\end{aligned}
\tag{3.1}
$$

We then substitute (2.6) and (2.7) into (3.1) to obtain the *1-D semi-discrete central-upwind scheme*:

$$
\frac{d}{dt}\bar{\mathbf{u}}_j(t) = -\frac{\mathbf{H}_{j+\frac{1}{2}}(t) - \mathbf{H}_{j-\frac{1}{2}}(t)}{\Delta x},
\tag{3.2}
$$

with the numerical flux $\mathbf{H}_{j+1/2}$, given by

$$
\mathbf{H}_{j+\frac{1}{2}}(t) := \frac{a_{j+\frac{1}{2}}^+ \mathbf{f}(\mathbf{u}_{j+\frac{1}{2}}^-) - a_{j+\frac{1}{2}}^- \mathbf{f}(\mathbf{u}_{j+\frac{1}{2}}^+)}{a_{j+\frac{1}{2}}^+ - a_{j+\frac{1}{2}}^-} + a_{j+\frac{1}{2}}^+ a_{j+\frac{1}{2}}^- \left[\frac{\mathbf{u}_{j+\frac{1}{2}}^+ - \mathbf{u}_{j+\frac{1}{2}}^-}{a_{j+\frac{1}{2}}^+ - a_{j+\frac{1}{2}}^-} - \mathbf{q}_{j+\frac{1}{2}} \right].
\tag{3.3}
$$

Here, the one-sided local speeds $a_{j+1/2}^{\pm}$ are given by (2.4), and $\mathbf{u}_{j+1/2}^{\pm}$ are the corresponding left- and right-sided values of the piecewise linear reconstruction at $x = x_{j+1/2}$, (2.5). Finally, the "correction" term (which corresponds to the reduced, compared with the original semi-discrete central-upwind scheme from [13], numerical dissipation) is:

$$
\mathbf{q}_{j+\frac{1}{2}} = \frac{1}{2} \lim_{\Delta t \to 0} \left\{ \Delta t \mathbf{s}_{j+\frac{1}{2}}^{n+1} \right\} = \text{minmod} \left(\frac{\mathbf{u}_{j+\frac{1}{2}}^+ - \mathbf{w}_{j+\frac{1}{2}}^{\text{int}}}{a_{j+\frac{1}{2}}^+ - a_{j+\frac{1}{2}}^-}, \frac{\mathbf{w}_{j+\frac{1}{2}}^{\text{int}} - \mathbf{u}_{j+\frac{1}{2}}^-}{a_{j+\frac{1}{2}}^+ - a_{j+\frac{1}{2}}^-} \right),
\tag{3.4}
$$

where the intermediate values $\mathbf{w}_{j+1/2}^{\text{int}}$ are obtained as we pass to the limit in (2.6):

$$
\mathbf{w}_{j+\frac{1}{2}}^{\text{int}} = \lim_{\Delta t \to 0} \bar{\mathbf{w}}_{j+\frac{1}{2}}^{n+1} = \frac{a_{j+\frac{1}{2}}^+ \mathbf{u}_{j+\frac{1}{2}}^+ - a_{j+\frac{1}{2}}^- \mathbf{u}_{j+\frac{1}{2}}^- - \left\{ \mathbf{f}(\mathbf{u}_{j+\frac{1}{2}}^+) - \mathbf{f}(\mathbf{u}_{j+\frac{1}{2}}^-) \right\}}{a_{j+\frac{1}{2}}^+ - a_{j+\frac{1}{2}}^-}.
\tag{3.5}
$$

Remark 3.1. The only difference between the new scheme (3.2)–(3.5) and the original semi-discrete central-upwind scheme in [13] is in the nonzero "correction" term $\mathbf{q}_{j+1/2}$ in the numerical flux (3.3). As one can easily verify, the sign of $\mathbf{q}_{j+1/2}$ always coincide

with the sign of $\frac{\mathbf{u}_{j+1/2}^{+}-\mathbf{u}_{j+1/2}^{-}}{a_{j+1/2}^{+}-a_{j+1/2}^{-}}$. Thus the "correction" term $\mathbf{q}_{j+1/2}$ is, in fact, a built-in anti-diffusion term. The source of this term is a more accurate projection step, described in Section 2, which is reflected in the semi-discrete version of our scheme as well. Being able to carry the anti-diffusion term from the fully-discrete scheme to its semi-discrete version allows one to minimize the loss of resolution, which is unavoidable when a more accurate, but rather complicated fully-discrete scheme is replaced with a less accurate, but much simpler semi-discrete one.

Remark 3.2. We would like to point out that no additional flux function evaluations are required in computing the anti-diffusion term $\mathbf{q}_{j+1/2}$ since the flux values used in (3.5), $\mathbf{f}(\mathbf{u}_{j+1/2}^{+})$ and $\mathbf{f}(\mathbf{u}_{j+1/2}^{-})$, are the same ones used in the computation of the first term of the numerical flux (3.3). Therefore, an extra computational cost related to the new anti-diffusion term is minimal.

Remark 3.3. As it has been recently proved in [2], in the scalar case, the numerical flux (3.3)–(3.5) is monotone, provided $f \in C^2$ is convex and satisfies two technical assumptions (see [2] for details).

Remark 3.4. The semi-discretization (3.2)–(3.5) results in a system of ODEs, which should be solved numerically by a stable ODE solver of an appropriate order. In the numerical examples, we have used the third-order strong stability preserving (SSP) Runge-Kutta method from [4].

Remark 3.5. One may add another degree of freedom by introducing a parameter, responsible for the sharpness of the piecewise linear reconstruction (2.9), in the computation of $\mathbf{q}_{j+1/2}$, namely, by setting

$$\mathbf{q}_{j+\frac{1}{2}} = \alpha \cdot \text{minmod} \left(\frac{\mathbf{u}_{j+\frac{1}{2}}^{+} - \mathbf{w}_{j+\frac{1}{2}}^{\text{int}}}{a_{j+\frac{1}{2}}^{+} - a_{j+\frac{1}{2}}^{-}}, \frac{\mathbf{w}_{j+\frac{1}{2}}^{\text{int}} - \mathbf{u}_{j+\frac{1}{2}}^{-}}{a_{j+\frac{1}{2}}^{+} - a_{j+\frac{1}{2}}^{-}} \right), \quad \alpha \in [0,1]. \tag{3.6}$$

Then, (3.2)–(3.3),(3.5)–(3.6) is, in fact, a *one-parameter family* of semi-discrete central-upwind schemes, in which larger the α smaller the amount of numerical dissipation. For example, the most dissipative choice ($\alpha = 0$) corresponds to the original central-upwind scheme from [13]. In the numerical experiments, presented in Section 5, we have taken $\alpha = 1$, but since high-order Godunov-type schemes are only essentially non-oscillatory, one may occasionally decrease α in order to increase the dissipation and reduce the amplitude of the so-called ENO-type oscillations. At the same time, the (formal) order of the scheme is independent of α and is determined only by the order of the piecewise polynomial reconstruction $\widetilde{\mathbf{u}}$, used to compute the values $\mathbf{u}_{j+1/2}^{\pm}$, and the order of the ODE solver.

4 Two-dimensional semi-discrete scheme

In this section, we extend the semi-discrete central-upwind scheme from Section 3 to two space dimensions. Let us consider the 2-D system of hyperbolic conservation laws:

$$\mathbf{u}_t + \mathbf{f}(\mathbf{u})_x + \mathbf{g}(\mathbf{u})_y = 0. \tag{4.1}$$

In the case of more than one space dimensions, the fully-discrete central-upwind scheme seems to be too complicated. Therefore, we proceed directly with the derivation of the semi-discrete scheme along the lines of [13].

Similarly to the 1-D case, we consider a uniform grid: $x_\alpha := \alpha \Delta x$, $y_\beta := \beta \Delta y$, $\Delta t := t^{n+1} - t^n$, and denote by $\bar{\mathbf{u}}_{j,k}^n \approx \frac{1}{\Delta x \Delta y} \int_{x_{j-1/2}}^{x_{j+1/2}} \int_{y_{k-1/2}}^{y_{k+1/2}} \mathbf{u}(x,y,t^n) dx dy$ the computed cell averages at time $t = t^n$.

Prior to evolving the computed solution in time, we reconstruct a piecewise linear interpolant

$$\widetilde{\mathbf{u}}(x,y,t^n) = \sum_{j,k} [\bar{\mathbf{u}}_{j,k}^n + (\mathbf{u}_x)_{j,k}^n (x - x_j) + (\mathbf{u}_y)_{j,k}^n (y - y_k)] \chi_{j,k}(x,y). \tag{4.2}$$

Here, $\chi_{j,k}(x,y)$ is the characteristic function over the corresponding cell $(x_{j-1/2}, x_{j+1/2}) \times (y_{k-1/2}, y_{k+1/2})$, and $(\mathbf{u}_x)_{j,k}^n$ and $(\mathbf{u}_y)_{j,k}^n$ stand for an (at least first-order) approximation of the x- and y-derivatives of $\mathbf{u}$ at the cell centers (x_j, y_k) at time $t = t^n$. In order to avoid oscillations, these partial derivatives must be computed with the help of a nonlinear limiter, for example, the generalized minmod limiter (2.3):

$$(\mathbf{u}_x)_{j,k}^n = \text{minmod}\left(\theta \frac{\bar{\mathbf{u}}_{j+1,k}^n - \bar{\mathbf{u}}_{j,k}^n}{\Delta x}, \frac{\bar{\mathbf{u}}_{j+1,k}^n - \bar{\mathbf{u}}_{j-1,k}^n}{2\Delta x}, \theta \frac{\bar{\mathbf{u}}_{j,k}^n - \bar{\mathbf{u}}_{j-1,k}^n}{\Delta x} \right),$$

$$\theta \in [1,2]. \tag{4.3}$$

$$(\mathbf{u}_y)_{j,k}^n = \text{minmod}\left(\theta \frac{\bar{\mathbf{u}}_{j,k+1}^n - \bar{\mathbf{u}}_{j,k}^n}{\Delta y}, \frac{\bar{\mathbf{u}}_{j,k+1}^n - \bar{\mathbf{u}}_{j,k-1}^n}{2\Delta y}, \theta \frac{\bar{\mathbf{u}}_{j,k}^n - \bar{\mathbf{u}}_{j,k-1}^n}{\Delta y} \right),$$

The evolution is then performed by integrating equation (4.1) over the nonuniform control volumes $D_{j,k}, D_{j+1/2,k}, D_{j,k+1/2}$ and $D_{j+1/2,k+1/2}$, outlined in Fig. 3. These domains are determined based on the one-sided local speeds of propagation (see [13] for details), which, in the convex case, can be estimated, for example, by:

$$a_{j+\frac{1}{2},k}^+ := \max\left\{ \lambda_N \left(A(\mathbf{u}_{j+1,k}^W) \right), \lambda_N \left(A(\mathbf{u}_{j,k}^E) \right), 0 \right\},$$

$$b_{j,k+\frac{1}{2}}^+ := \max\left\{ \lambda_N \left(B(\mathbf{u}_{j,k+1}^S) \right), \lambda_N \left(B(\mathbf{u}_{j,k}^N) \right), 0 \right\},$$

$$a_{j+\frac{1}{2},k}^- := \min\left\{ \lambda_1 \left(A(\mathbf{u}_{j+1,k}^W) \right), \lambda_1 \left(A(\mathbf{u}_{j,k}^E) \right), 0 \right\}, \tag{4.4}$$

$$b_{j,k+\frac{1}{2}}^- := \min\left\{ \lambda_1 \left(B(\mathbf{u}_{j,k+1}^S) \right), \lambda_1 \left(B(\mathbf{u}_{j,k}^N) \right), 0 \right\}.$$
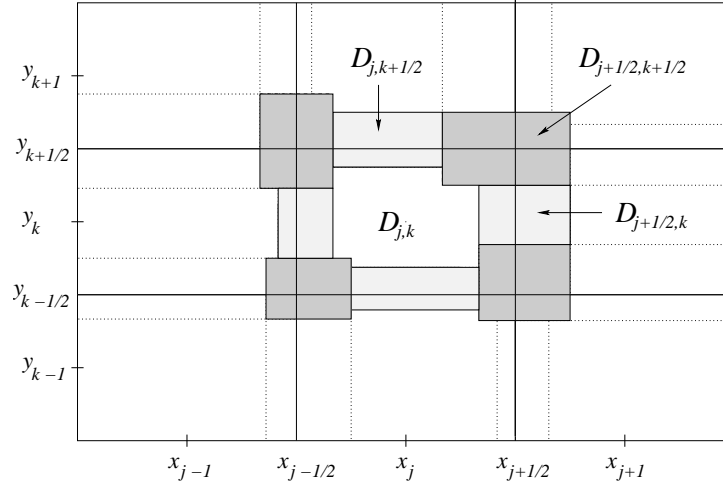
Figure 3: Nonuniform control volumes in the 2-D set-up.

Here, $\lambda_1 < \lambda_2 < \ldots < \lambda_N$ are the N eigenvalues of the corresponding Jacobians, $A := \partial \mathbf{f} / \partial \mathbf{u}$ and $B := \partial \mathbf{g} / \partial \mathbf{u}$, and the point values of the piecewise linear reconstruction (4.2) are given by:

$$\mathbf{u}_{j,k}^{\mathrm{E(W)}} := \bar{\mathbf{u}}_{j,k}^n \pm \frac{\Delta x}{2} (\mathbf{u}_x)_{j,k}^n, \quad \mathbf{u}_{j,k}^{\mathrm{N(S)}} := \bar{\mathbf{u}}_{j,k}^n \pm \frac{\Delta y}{2} (\mathbf{u}_y)_{j,k}^n. \tag{4.5}$$

We refer the reader to [13, 18] for the details.

After the evolution step, the solution at time $t = t^{n+1}$ will be realized by the intermediate cell averages $\{\bar{\mathbf{w}}_{j,k}^{n+1}\}$, $\{\bar{\mathbf{w}}_{j+1/2,k}^{n+1}\}$, $\{\bar{\mathbf{w}}_{j,k+1/2}^{n+1}\}$ and $\{\bar{\mathbf{w}}_{j+1/2,k+1/2}^{n+1}\}$ over the corresponding domains D. To complete the step of a fully-discrete scheme, we will then need to project these data back onto the original grid. This will require another piecewise linear reconstruction:

$$\widetilde{\mathbf{w}}^{n+1}(x,y) := \sum_{j,k} \Big[\widetilde{\mathbf{w}}_{j,k}^{n+1}(x,y) \chi_{D_{j,k}}(x,y) + \widetilde{\mathbf{w}}_{j+\frac{1}{2},k}^{n+1}(x,y) \chi_{D_{j+\frac{1}{2},k}}(x,y)$$

$$+ \widetilde{\mathbf{w}}_{j,k+\frac{1}{2}}^{n+1}(x,y) \chi_{D_{j,k+\frac{1}{2}}}(x,y) + \widetilde{\mathbf{w}}_{j+\frac{1}{2},k+\frac{1}{2}}^{n+1}(x,y) \chi_{D_{j+\frac{1}{2},k+\frac{1}{2}}}(x,y) \Big], \tag{4.6}$$

where $\{\widetilde{\mathbf{w}}_{j,k}^{n+1}(x,y), \widetilde{\mathbf{w}}_{j+1/2,k}^{n+1}(x,y), \widetilde{\mathbf{w}}_{j,k+1/2}^{n+1}(x,y)$ and $\widetilde{\mathbf{w}}_{j+1/2,k+1/2}^{n+1}(x,y)\}$ are the corresponding linear pieces, and the χ's stand for the characteristic functions of the corresponding domains D.

The linear pieces over the side domains, $D_{j+1/2,k}$ and $D_{j,k+1/2}$, should be carefully chosen in order to reduce numerical dissipation (compared with the schemes in [13, 18]). For instance, let us consider a typical side domain $D_{j+1/2,k}$, whose corners are denoted by P_1, P_2, P_3, and P_4, see Fig. 4. Since the length of its x-side is proportional to Δt, namely, $|P_2 - P_1| = |P_4 - P_3| = (a_{j+1/2,k}^+ - a_{j+1/2,k}^-)\Delta t$, the x-slope of the corresponding linear piece, $(\mathbf{w}_x)_{j+1/2,k}^{n+1}$, should be proportional to $\Delta \mathbf{w} / \Delta t$ rather than to $\Delta \mathbf{w} / \Delta x$. This can be
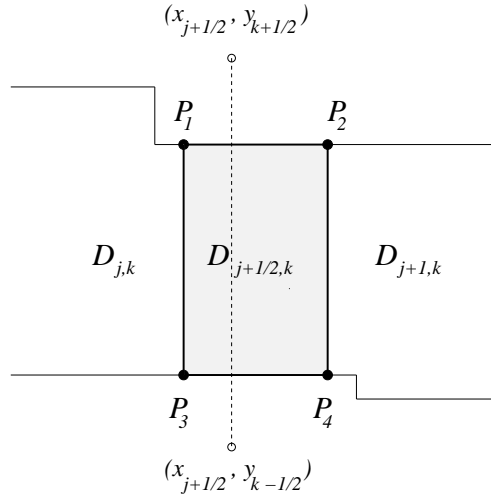
Figure 4: The side domain $D_{j+1/2,k}$.

achieved by a complete analogy with the 1-D case. We first use the Taylor expansions to predict the values of the solution at the corners of $D_{j+1/2,k}$:

$$\mathbf{u}^{n+1}(P_i) = \widetilde{\mathbf{u}}(P_i, t^n) - \Delta t \left[\mathbf{f}(\widetilde{\mathbf{u}}(P_i, t^n))_x + \mathbf{g}(\widetilde{\mathbf{u}}(P_i, t^n))_y \right], \quad i = 1,2,3,4.$$

If any of these values, say $\mathbf{u}^{n+1}(P_{i_0})$ is not between the cell averages $\bar{\mathbf{w}}_{j,k}^{n+1}$ and $\bar{\mathbf{w}}_{j+1,k}^{n+1}$, we would prevent oscillation by setting

$$\mathbf{u}^{n+1}(P_{i_0}) := \begin{cases} \bar{\mathbf{w}}_{j,k}^{n+1}, & \text{if } i_0 = 1 \text{ or } 3, \\[2mm] \bar{\mathbf{w}}_{j+1,k}^{n+1}, & \text{if } i_0 = 2 \text{ or } 4. \end{cases}$$

Using the evolved values at the corners, we construct a piecewise linear interpolant over the domain $D_{j+1/2,k}$:

$$\bar{\mathbf{w}}_{j+\frac{1}{2},k}^{n+1} + (\mathbf{u}_x)_{j+\frac{1}{2},k}^{n+1}(x - x_{j+\frac{1}{2},k}^{n+1}) + (\mathbf{u}_y)_{j+\frac{1}{2},k}^{n+1}(y - y_{j+\frac{1}{2},k}^{n+1}),$$

where

$$x_{j+\frac{1}{2},k}^{n+1} := x_{j+\frac{1}{2}} + \frac{a_{j+\frac{1}{2},k}^- + a_{j+\frac{1}{2},k}^+}{2}\Delta t$$

and

$$y_{j+\frac{1}{2},k}^{n+1} := y_k + \frac{\min(b_{j,k+\frac{1}{2}}^-, b_{j+1,k+\frac{1}{2}}^-) + \max(b_{j,k-\frac{1}{2}}^+, b_{j+1,k-\frac{1}{2}}^+)}{2}\Delta t$$

are the coordinates of the center of $D_{j+1/2,k}$, and $(\mathbf{u}_x)_{j+1/2,k}^{n+1}$ and $(\mathbf{u}_y)_{j+1/2,k}^{n+1}$ are the x- and y-slopes that are to be computed with the help of a nonlinear limiter.

In fact, only the x-slope, $(\mathbf{u}_x)_{j+1/2,k}^{n+1}$, should be carefully selected since in the y-direction, the size of $D_{j+1/2,k}$ is proportional to Δy and therefore, after passing to the semi-discrete limit we obtain: $\{\Delta t(\mathbf{u}_y)_{j+1/2,k}^{n+1}\} \to \mathbf{0}$ as $\Delta t \to 0$. A sharp non-oscillatory reconstruction is obtained by taking

$$(\mathbf{u}_x)_{j+\frac{1}{2},k}^{n+1} = \text{minmod}\left(\frac{\mathbf{u}^{n+1}(P_2) - \bar{\mathbf{w}}_{j+\frac{1}{2},k}^{n+1}}{\delta}, \frac{\bar{\mathbf{w}}_{j+\frac{1}{2},k}^{n+1} - \mathbf{u}^{n+1}(P_1)}{\delta}, \frac{\mathbf{u}^{n+1}(P_4) - \bar{\mathbf{w}}_{j+\frac{1}{2},k}^{n+1}}{\delta},\right.$$
$$\left.\frac{\bar{\mathbf{w}}_{j+\frac{1}{2},k}^{n+1} - \mathbf{u}^{n+1}(P_3)}{\delta}\right), \quad \delta := \frac{|P_2 - P_1|}{2} = \frac{\Delta t}{2}(a_{j+\frac{1}{2},k}^+ - a_{j+\frac{1}{2},k}^-).$$

This slope selection helps to prevent oscillations at the corners of $D_{j+1/2,k}$, which is enough to make the piecewise linear reconstruction (4.6) non-oscillatory.

We note that a piecewise linear reconstruction over $D_{j,k+1/2}$ is obtained in a similar way, a piecewise linear reconstruction over $D_{j,k}$ will always be averaged out, and no particulars of the piecewise linear reconstruction over the corner domains $D_{j+1/2,k+1/2}$ will affect the resulting semi-discrete scheme (see [13] for details).

As we have mentioned in the beginning of this section, we are only interested in the 2-D semi-discrete central-upwind scheme. Therefore, instead of completing the derivation of the 2-D fully-discrete scheme, we proceed by passing to the semi-discrete limit ($\Delta t \to 0$) along the lines of [13]. The resulting new *2-D semi-discrete central-upwind scheme* is then obtained in the following flux form:

$$\frac{d}{dt}\bar{\mathbf{u}}_{j,k}(t) = -\frac{\mathbf{H}_{j+\frac{1}{2},k}^x(t) - \mathbf{H}_{j-\frac{1}{2},k}^x(t)}{\Delta x} - \frac{\mathbf{H}_{j,k+\frac{1}{2}}^y(t) - \mathbf{H}_{j,k-\frac{1}{2}}^y(t)}{\Delta y}, \tag{4.7}$$

where the *second-order numerical fluxes* are:

$$\mathbf{H}_{j+\frac{1}{2},k}^x(t) := \frac{a_{j+\frac{1}{2},k}^+ \mathbf{f}(\mathbf{u}_{j,k}^{\text{E}}) - a_{j+\frac{1}{2},k}^- \mathbf{f}(\mathbf{u}_{j+1,k}^{\text{W}})}{a_{j+\frac{1}{2},k}^+ - a_{j+\frac{1}{2},k}^-} + a_{j+\frac{1}{2},k}^+ a_{j+\frac{1}{2},k}^- \left[\frac{\mathbf{u}_{j+1,k}^{\text{W}} - \mathbf{u}_{j,k}^{\text{E}}}{a_{j+\frac{1}{2},k}^+ - a_{j+\frac{1}{2},k}^-} - \mathbf{q}_{j+\frac{1}{2},k}^x\right], \tag{4.8}$$

and

$$\mathbf{H}_{j,k+\frac{1}{2}}^y(t) := \frac{b_{j,k+\frac{1}{2}}^+ \mathbf{g}(\mathbf{u}_{j,k}^{\text{N}}) - b_{j,k+\frac{1}{2}}^- \mathbf{g}(\mathbf{u}_{j,k+1}^{\text{S}})}{b_{j,k+\frac{1}{2}}^+ - b_{j,k+\frac{1}{2}}^-} + b_{j,k+\frac{1}{2}}^+ b_{j,k+\frac{1}{2}}^- \left[\frac{\mathbf{u}_{j,k+1}^{\text{S}} - \mathbf{u}_{j,k}^{\text{N}}}{b_{j,k+\frac{1}{2}}^+ - b_{j,k+\frac{1}{2}}^-} - \mathbf{q}_{j,k+\frac{1}{2}}^y\right]. \tag{4.9}$$

Similarly to the 1-D case, we will refer to $\mathbf{q}_{j+1/2,k}^x$ and $\mathbf{q}_{j,k+1/2}^y$ as the built-in anti-diffusion

terms. They are given by:

$$\mathbf{q}^x_{j+\frac{1}{2},k} = \frac{1}{2} \lim_{\Delta t \to 0} \left\{ \Delta t (\mathbf{u}_x)^{n+1}_{j+\frac{1}{2},k} \right\} \tag{4.10}$$

$$= \mathrm{minmod} \left(\frac{\mathbf{u}^{\mathrm{NW}}_{j+1,k} - \mathbf{w}^{\mathrm{int}}_{j+\frac{1}{2},k}}{a^+_{j+\frac{1}{2},k} - a^-_{j+\frac{1}{2},k}}, \frac{\mathbf{w}^{\mathrm{int}}_{j+\frac{1}{2},k} - \mathbf{u}^{\mathrm{NE}}_{j,k}}{a^+_{j+\frac{1}{2},k} - a^-_{j+\frac{1}{2},k}}, \frac{\mathbf{u}^{\mathrm{SW}}_{j+1,k} - \mathbf{w}^{\mathrm{int}}_{j+\frac{1}{2},k}}{a^+_{j+\frac{1}{2},k} - a^-_{j+\frac{1}{2},k}}, \frac{\mathbf{w}^{\mathrm{int}}_{j+\frac{1}{2},k} - \mathbf{u}^{\mathrm{SE}}_{j,k}}{a^+_{j+\frac{1}{2},k} - a^-_{j+\frac{1}{2},k}} \right),$$

$$\mathbf{q}^y_{j,k+\frac{1}{2}} = \frac{1}{2} \lim_{\Delta t \to 0} \left\{ \Delta t (\mathbf{u}_y)^{n+1}_{j,k+\frac{1}{2}} \right\} \tag{4.11}$$

$$= \mathrm{minmod} \left(\frac{\mathbf{u}^{\mathrm{SW}}_{j,k+1} - \mathbf{w}^{\mathrm{int}}_{j,k+\frac{1}{2}}}{b^+_{j,k+\frac{1}{2}} - b^-_{j,k+\frac{1}{2}}}, \frac{\mathbf{w}^{\mathrm{int}}_{j,k+\frac{1}{2}} - \mathbf{u}^{\mathrm{NW}}_{j,k}}{b^+_{j,k+\frac{1}{2}} - b^-_{j,k+\frac{1}{2}}}, \frac{\mathbf{u}^{\mathrm{SE}}_{j,k+1} - \mathbf{w}^{\mathrm{int}}_{j,k+\frac{1}{2}}}{b^+_{j,k+\frac{1}{2}} - b^-_{j,k+\frac{1}{2}}}, \frac{\mathbf{w}^{\mathrm{int}}_{j,k+\frac{1}{2}} - \mathbf{u}^{\mathrm{NE}}_{j,k}}{b^+_{j,k+\frac{1}{2}} - a^-_{j,k+\frac{1}{2}}} \right),$$

where the intermediate values are:

$$\mathbf{w}^{\mathrm{int}}_{j+\frac{1}{2},k} = \lim_{\Delta t \to 0} \bar{\mathbf{w}}^{n+1}_{j+\frac{1}{2},k} = \frac{a^+_{j+\frac{1}{2},k} \mathbf{u}^{\mathrm{W}}_{j+1,k} - a^-_{j+\frac{1}{2},k} \mathbf{u}^{\mathrm{E}}_{j,k} - \left\{ \mathbf{f}(\mathbf{u}^{\mathrm{W}}_{j+1,k}) - \mathbf{f}(\mathbf{u}^{\mathrm{E}}_{j,k}) \right\}}{a^+_{j+\frac{1}{2},k} - a^-_{j+\frac{1}{2},k}}, \tag{4.12}$$

$$\mathbf{w}^{\mathrm{int}}_{j,k+\frac{1}{2}} = \lim_{\Delta t \to 0} \bar{\mathbf{w}}^{n+1}_{j,k+\frac{1}{2}} = \frac{b^+_{j,k+\frac{1}{2}} \mathbf{u}^{\mathrm{S}}_{j,k+1} - b^-_{j,k+\frac{1}{2}} \mathbf{u}^{\mathrm{N}}_{j,k} - \left\{ \mathbf{g}(\mathbf{u}^{\mathrm{S}}_{j,k+1}) - \mathbf{g}(\mathbf{u}^{\mathrm{N}}_{j,k}) \right\}}{b^+_{j,k+\frac{1}{2}} - b^-_{j,k+\frac{1}{2}}}, \tag{4.13}$$

and $\mathbf{u}^{\mathrm{NE}}_{j,k}$, $\mathbf{u}^{\mathrm{NW}}_{j,k}$, $\mathbf{u}^{\mathrm{SE}}_{j,k}$ and $\mathbf{u}^{\mathrm{SW}}_{j,k}$ are the corresponding corner point values of the piecewise linear reconstruction (4.2) in the (j,k)th cell:

$$\mathbf{u}^{\mathrm{NE(NW)}}_{j,k} := \bar{\mathbf{u}}^n_{j,k} \pm \frac{\Delta x}{2} (\mathbf{u}_x)^n_{j,k} + \frac{\Delta y}{2} (\mathbf{u}_y)^n_{j,k}, \quad \mathbf{u}^{\mathrm{SE(SW)}}_{j,k} := \bar{\mathbf{u}}^n_{j,k} \pm \frac{\Delta x}{2} (\mathbf{u}_x)^n_{j,k} - \frac{\Delta y}{2} (\mathbf{u}_y)^n_{j,k}. \tag{4.14}$$

Remark 4.1. Note that we are interested in the second-order scheme, and thus Simpson's rule, used in the evaluation of the spatial integrals in [13], has been replaced with the second-order midpoint rule (see also [18]). However, our 2-D scheme (4.7)–(4.13) is still genuinely multidimensional since the computation of the anti-diffusion terms $\mathbf{q}^x_{j+1/2,k}$ and $\mathbf{q}^y_{j,k+1/2}$ cannot be carried out in the "dimension-by-dimension" manner.

Remark 4.2. As in the 1-D case, the only difference between the new 2-D central-upwind scheme and the 2-D second-order scheme from [13] is in the anti-diffusion terms $\mathbf{q}^x_{j+1/2,k}$ and $\mathbf{q}^y_{j,k+1/2}$ in (4.8) and (4.9), respectively. These terms help to reduce the numerical dissipation present in the original semi-discrete central-upwind scheme in [13, 18]. Yet, when multidimensional systems are solved, one cannot completely avoid oscillations, and if their size gets larger than it would be acceptable, one may increase the dissipation a little bit by multiplying $\mathbf{q}^x_{j+1/2,k}$ and $\mathbf{q}^y_{j,k+1/2}$ by a constant $\alpha \in [0,1)$ similarly to (3.6).

Remark 4.3. We would like to emphasize that, as in the 1-D case, no additional flux function evaluations are required in computing the anti-diffusion terms since the flux

values used in (4.12)–(4.13), $\mathbf{f}(\mathbf{u}^W_{j+1,k})$, $\mathbf{f}(\mathbf{u}^E_{j,k})$, $\mathbf{g}(\mathbf{u}^S_{j,k+1})$ and $\mathbf{g}(\mathbf{u}^N_{j,k})$, are the same ones used in the computation of the first terms of the numerical fluxes (4.8) and (4.9). Therefore, in the 2-D case, an extra computational cost related to the new anti-diffusion terms is small as well.

Remark 4.4. The system of ODEs (4.7) should be solved by a stable ODE solver. In our numerical experiments, we have used the third-order SSP Runge-Kutta method.

5 Numerical experiments

In this section, we illustrate the performance of the new second-order semi-discrete central-upwind schemes (NEW) on a number of 1-D and 2-D examples. We also compare its performance with the original central-schemes schemes (OLD) from [13, 18].

In Section 5.1 and Section 5.2 below, we present numerical solutions of the Euler equations of gas dynamics for ideal gases, which in the 2-D case read:

$$\frac{\partial}{\partial t}\begin{bmatrix} \rho \\ \rho u \\ \rho v \\ E \end{bmatrix} + \frac{\partial}{\partial x}\begin{bmatrix} \rho u \\ \rho u^2 + p \\ \rho uv \\ u(E+p) \end{bmatrix} + \frac{\partial}{\partial y}\begin{bmatrix} \rho v \\ \rho uv \\ \rho v^2 + p \\ v(E+p) \end{bmatrix} = 0,$$

$$p = (\gamma-1)\left[E - \frac{\rho}{2}(u^2+v^2)\right]. \tag{5.1}$$

Here, ρ, u, v, p and E are the density, the x- and y-velocities, the pressure and the total energy, respectively. In all the examples below, we take $\gamma = 1.4$.

5.1 One-dimensional Euler equations of gas dynamics

We first test our new 1-D second-order semi-discrete central-upwind scheme (3.2)–(3.5), (2.3)–(2.5) on the 1-D Euler equations of gas dynamics. The second-order scheme employs the minmod limiter (2.3) with $\theta = 1$, while the first-order scheme is obtained by setting the slopes in (2.5) to be zero. The OLD schemes are obtained by setting $\mathbf{q}_{j+1/2} = \mathbf{0}$ in (3.3).

Example 1: Moving contact wave
In this example, we apply the NEW and the OLD central-upwind schemes to the 1-D Euler system with the Riemann initial data:

$$(\rho,u,p)(x,0) = \begin{cases} (1.4,0.1,1), & x < 0.5, \\ (1.0,0.1,1), & x > 0.5, \end{cases}$$

which correspond to an isolated contact discontinuity: the exact solution is just the initial data shifted by $0.1t$ to the right of $x = 0.5$. We first compute the approximate solution up to time $t = 2$, using the uniform grid with $\Delta x = 1/200$. In Fig. 5, we show the density
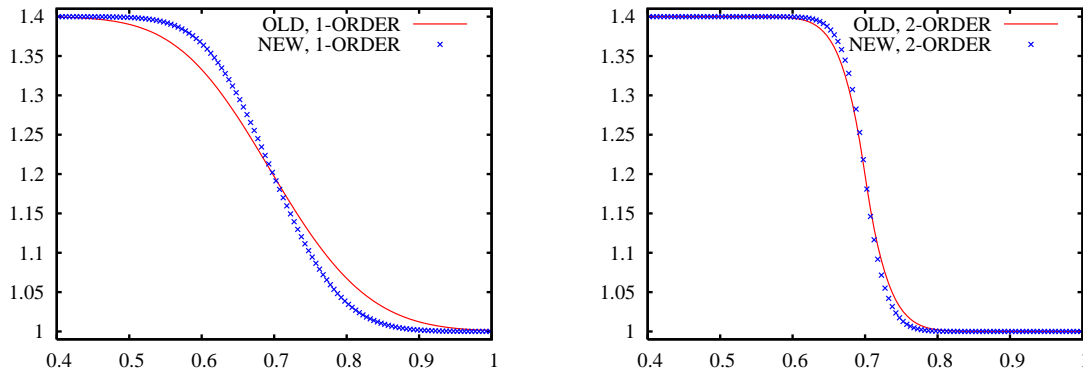
Figure 5: Isolated contact by the NEW and OLD first-order (left) and second-order (right) schemes using the same spatial grid.
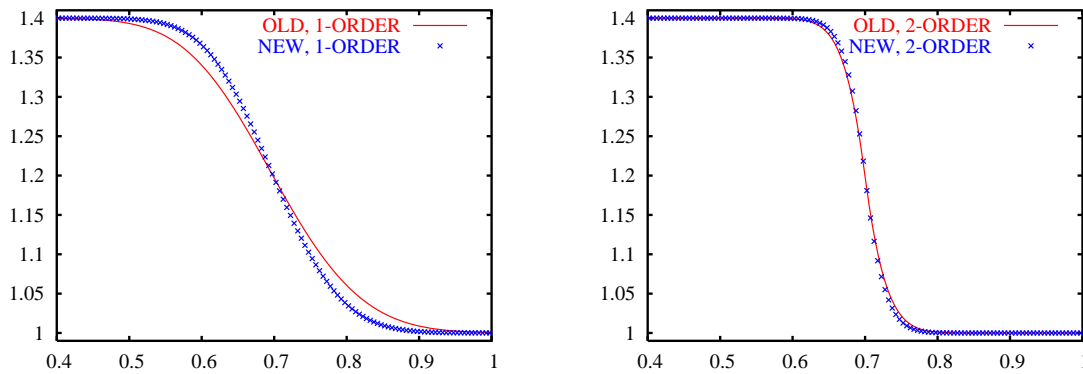

Figure 6: Isolated contact by the NEW and OLD first-order (left) and second-order (right) schemes using the same CPU time.

plots obtained by both the NEW and the OLD schemes at time $t = 2$. Near the location of discontinuity, the density profiles obtained by the NEW schemes are clearly sharper than the ones computed by the corresponding OLD schemes. The difference is especially large in the first-order calculations, presented in Fig. 5 (left). When the second-order piecewise linear reconstruction is used to increase the resolution, the difference in the results obtained by the NEW and the OLD schemes becomes smaller (as expected), but still clearly visible, see Fig. 5 (right).

We then perform a more thorough comparison between the NEW and the OLD schemes by taking into account additional computational cost of the NEW scheme due to the necessity to calculate the anti-diffusion term $\mathbf{q}_{j+1/2}$ in (3.4)–(3.5). To this end, we measure the CPU time spent on the above calculations by the NEW first- and second-order schemes and refine the mesh used by the corresponding OLD schemes so that exactly the same CPU time is spent to compute the numerical solutions at $t = 2$ (the size of the

uniform grid is then $\Delta x = 1/232$ for the OLD first-order scheme and $\Delta x = 1/236$ for the OLD second-order scheme). The results are shown in Fig. 6, where one can clearly see that the NEW schemes achieve a better resolution.

Remark 5.1. We would like to point out that the first-order versions of both the NEW and the OLD schemes are obtained by setting all the slopes $\mathbf{s}_j^n = \mathbf{0}$ in the reconstruction (2.2), (2.5). Note, however, that using the piecewise constant interpolant at the reconstruction step does not cause the anti-diffusion term $\mathbf{q}_{j+1/2}$ to vanish and therefore the NEW first-order scheme is much less diffusive than the OLD one.

The first-order semi-discrete central-upwind scheme can be written in the same flux form (3.2)–(3.5) as the second-order one, but the reconstructed values $\mathbf{u}_{j+1/2}^+$ and $\mathbf{u}_{j+1/2}^-$ should be replaced by $\mathbf{u}_{j+1}$ and $\mathbf{u}_j$, respectively.

Example 2: Stationary contact wave and traveling shock and rarefaction

In this example, we solve the 1-D Euler system subject to another Riemann initial data:

$$(\rho,u,p)(x,0) = \left\{ \begin{array}{ll} (1,-19.59745,1000), & x < 0.8, \\ (1,-19.59745,0.01), & x > 0.8. \end{array} \right.$$

The exact solution of this initial-value problem consists of a stationary contact wave, a traveling shock and a traveling rarefaction wave. We use the uniform grid with $\Delta x = 1/200$ and compute the solution at a final time $t = 0.012$. The computed density is plotted in Fig. 7, which clearly demonstrates sharper resolution achieved by the NEW scheme in the neighborhood of the contact wave. Once again, the difference between the NEW and the OLD first-order results, Fig. 7 (left) is much more significant than between the second-order ones, Fig. 7 (right). The reference solution is obtained by the NEW second-order semi-discrete central-upwind scheme on a 12 times finer uniform grid with $\Delta x = 1/2400$.

Example 3:

In this example, we compute the solution of the 1-D Euler system subject to the following initial data:

$$(\rho,u,p)(x,0) = \left\{ \begin{array}{llll} (3.857143, & -0.920279, & 10.33333), & x < 0, \\ (1+\varepsilon\sin(5x), & -3.549648, & 1.00000), & 0 < x < 10, \\ (1.000000, & -3.549648, & 1.00000), & x \geq 10, \end{array} \right.$$

that correspond to a density perturbation running leftwards into a stationary shock of Mach number $M_s = 3$. This example, taken from [9], has a numerical "flavor" of an acoustic wave, propagating through a steady discontinuous flow field. We take $\varepsilon = 0.2$ and present the computed solutions at time $t = 2$.

Both solutions by the NEW and the OLD second-order schemes are obtained on the uniform grid with $\Delta x = 1/80$ and compared with a fine grid (with $\Delta x = 1/1000$) reference solution obtained by the NEW second-order scheme. The results are shown in Fig. 9, where one can clearly see the superiority of the resolution achieved by the NEW central-upwind scheme.
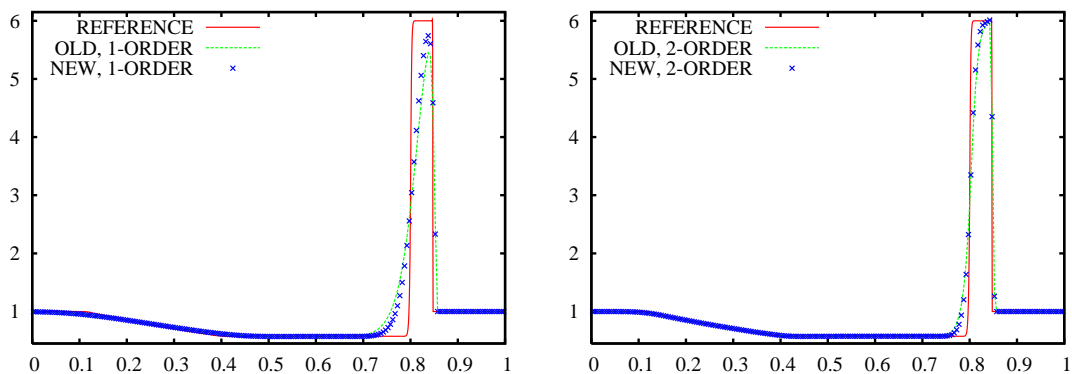
Figure 7: Example 2: density by the NEW and OLD first-order (left) and second-order (right) schemes.
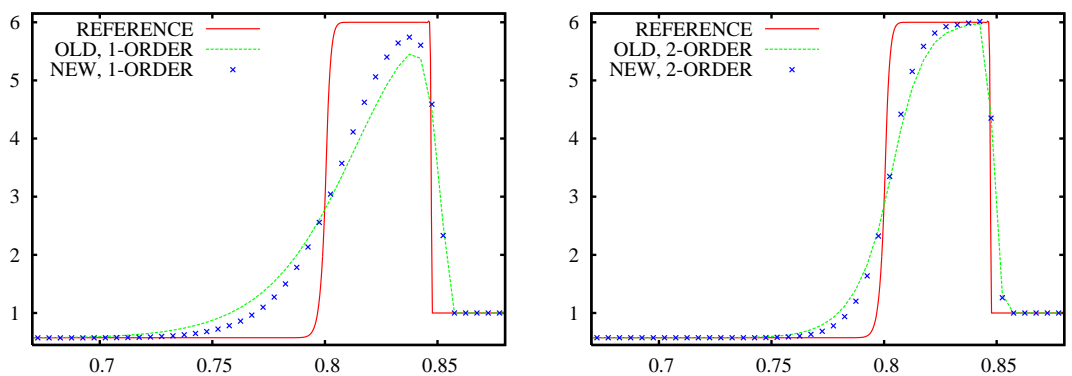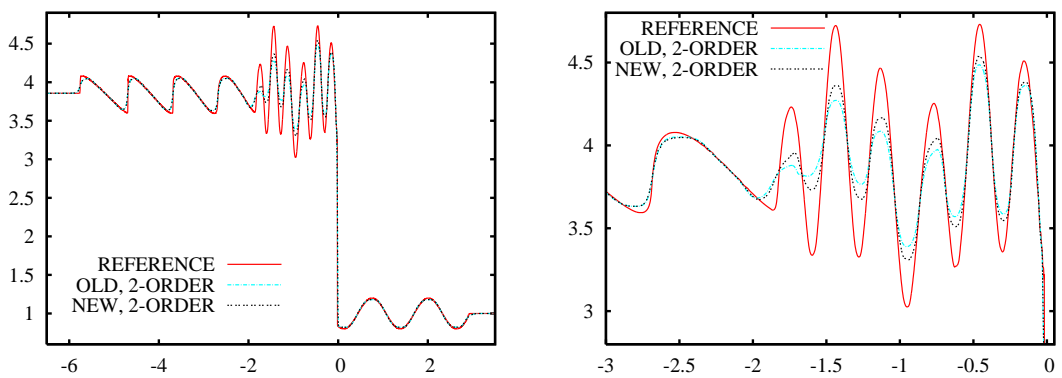
Figure 8: Same as Fig. 7 — zoom at $[0.67\!:\!0.88]$.

Figure 9: Example 3: density by the NEW and OLD second-order schemes (left); zoom at $[-3,0.05]$ (right).

5.2 Two-dimensional Euler equations of gas dynamics

In this section, we bring two 2-D numerical examples, in which one can clearly observe the effects of the reduced numerical dissipation in the NEW second-order semi-discrete central-upwind scheme (4.7)–(4.14),(4.3)–(4.5). In both examples, we have used the generalized minmod reconstruction (4.3) with $\theta = 1.5$. We also compare the NEW and the OLD central-upwind schemes. The latter scheme is obtained by setting $\mathbf{q}^x_{j+1/2,k}$ and $\mathbf{q}^y_{j,k+1/2}$ in (4.8) and(4.9), respectively.

Example 4: Shock-bubble interaction

We consider the 2-D Euler equation of gas dynamics (5.1) in the strip $\mathbb{R} \times [-0.5,0.5]$ with the solid wall boundary conditions prescribed at $y = \pm 0.5$. The initial data correspond to a vertical left-moving shock, initially located at $x = 0.75$, and a circular bubble with radius 0.25, initially located at the origin:

$$
(p,\rho,u,v)(x,y,0) = \begin{cases} \left(1,\dfrac{1}{29},0,0\right), & x^2 + y^2 < \dfrac{1}{16}, \\[2mm] \left(\dfrac{3}{2},\dfrac{4}{3},-\dfrac{707}{2000},0\right), & x > \dfrac{3}{4}, \\[2mm] (1,1,0,0), & \text{otherwise.} \end{cases} \tag{5.2}
$$

In Figs. 10–12, we show the density contour lines obtained by the NEW and the OLD schemes at times $t = 1$ and $t = 4$ (we have used the uniform grid with $\Delta x = \Delta y = 1/400$). By time $t = 4$ the bubble computed by the OLD scheme has already split into two parts. The splitting apparently caused by the numerical diffusion, and when the diffusion is reduced, no splitting has occurred by time $t = 4$ (see Figs. 11–12).

Example 5: Explosion

In the final example, we compute the so-called explosion problem proposed in [30] (see also [27], where different numerical schemes were tested on this problem). This is a radial symmetric 2-D problem with higher density and higher pressure inside the initial circular region of radius $r = 0.4$ centered at the origin (the physical domain is $[-1.5,1.5] \times [-1.5,1.5]$), which cause the explosion. Inside the circle, density and pressure are $\rho_{in} = 1$, $p_{in} = 1$, while in the rest of the domain $\rho_{out} = 0.1$ and $p_{out} = 0.1$. The gas is initially at rest ($u_{in} = v_{in} = u_{out} = v_{out} = 0$). We perform the computation in the first quadrant $[0,1.5] \times [0,1.5]$ using the uniform grid with $\Delta x = \Delta y = 3/800$ (Fig. 13) and $\Delta x = \Delta y = 3/1600$ (Fig. 14). The solution is shown at time $t = 3.2$, by which the circular contact curve typically developes instabilities (at smaller times, numerical diffusion present at non-oscillatory finite-volume schemes artificially stabilizes the contact curve). This example is a good test for the amount of numerical diffusion present in the NEW and the OLD schemes. One can clearly see, especially in the case of the finer mesh (Fig. 14), that the contact curve, computed by the NEW scheme, is "curlier" than the one captured by the OLD scheme. This is an effect of a reduced numerical dissipation.

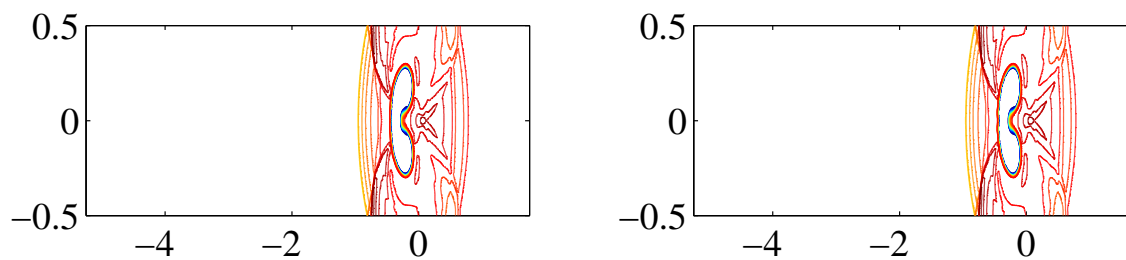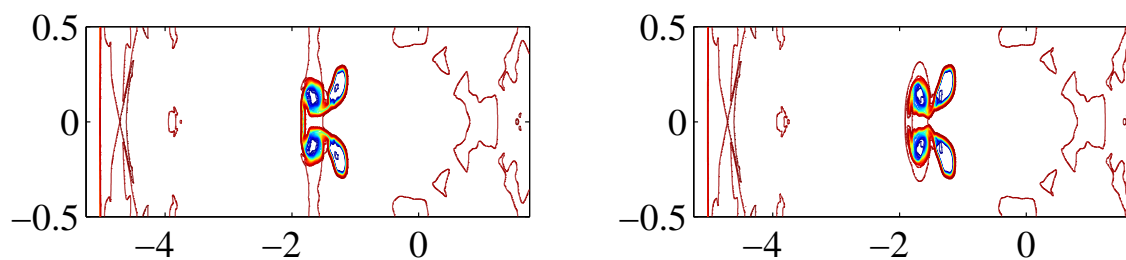Figure 10: Shock-bubble interaction: density by the NEW (left) and OLD (right) schemes at $t=1$.

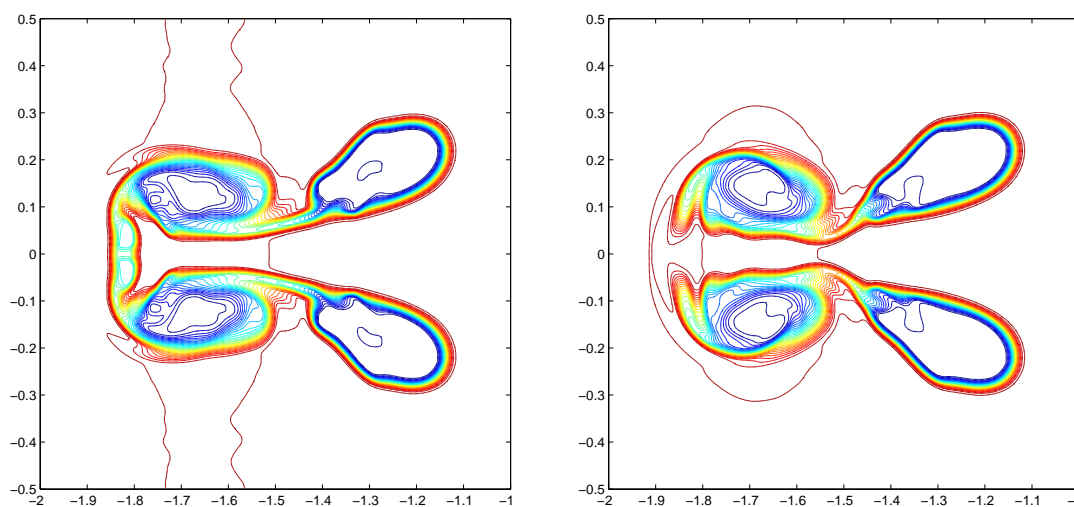Figure 11: Shock-bubble interaction: density by the NEW (left) and OLD (right) schemes at $t=4$.

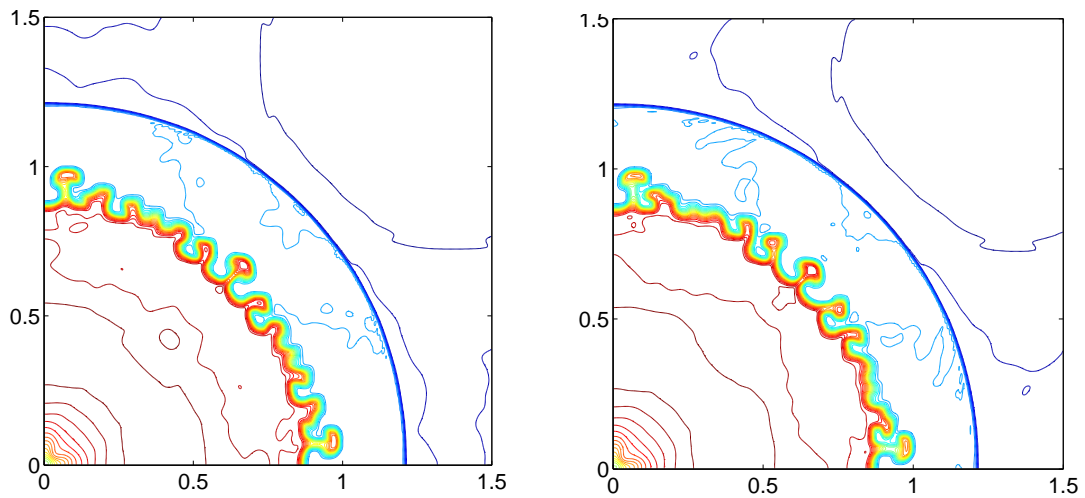Figure 12: Same as Fig. 11 — zoom at $[-2,-1]\times[-0.5,0.5]$.

Acknowledgments

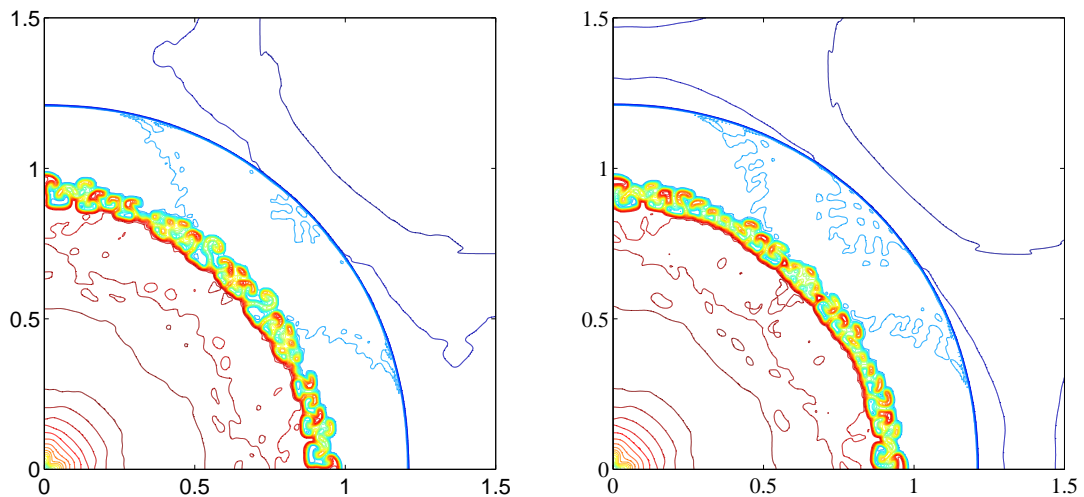Figure 13: Explosion: density by the NEW (left) and OLD (right) schemes with $\Delta x = \Delta y = 3/800$.

Figure 14: Explosion: density by the NEW (left) and OLD (right) schemes with $\Delta x = \Delta y = 3/1600$.

References

[1] P. Arminjon and M. C. Viallon, Généralisation du schéma de Nessyahu-Tadmor pour une équation hyperbolique à deux dimensions d'espace, CR Acad. Sci. Paris, Series I, 320 (1995), 85-88.

 [2] S. Bryson, A. Kurganov, D. Levy and G. Petrova, Semi-discrete central-upwind schemes with reduced dissipation for Hamilton-Jacobi equations, IMA J. Numer. Anal., 25 (2005), 113-138.
 [3] K. O. Friedrichs, Symmetric hyperbolic linear differential equations, Commun. Pur. Appl. Math., 7 (1954), 345-392.
 [4] S. Gottlieb, C. W. Shu and E. Tadmor, Strong stability-preserving high order time discretization methods, SIAM Rev., 43 (2001), 89-112.
 [5] A. Harten and S. Osher, Uniformly high-order accurate nonoscillatory schemes, I, SIAM J. Numer. Anal., 24 (1987), 279-309.
 [6] G. S. Jiang, D. Levy, C. T. Lin, S. Osher and E. Tadmor, High-resolution nonoscillatory central schemes with nonstaggered grids for hyperbolic conservation laws, SIAM J. Numer. Anal., 35 (1998), 2147-2168.
 [7] G. S. Jiang and E. Tadmor, Non-oscillatory central schemes for multidimensional hyperbolic conservation laws, SIAM J. Sci. Comput., 19 (1998), 1892-1917.
 [8] S. Karni, E. Kirr, A. Kurganov and G. Petrova, Compressible two-phase flows by central and upwind schemes, Math. Model. Numer. Anal., 38 (2004), 477-493.
 [9] S. Karni, A. Kurganov and G. Petrova, A smoothness indicator for adaptive algorithms for hyperbolic systems, J. Comput. Phys., 178 (2002), 323-341.
[10] A. Kurganov, Central-upwind schemes for balance laws. Application to the Broadwell model, in: R. Herbin and D. Kroener (Eds.), Proceedings of the Third International Symposium on Finite Volumes for Complex Applications, Porquerolles, 2002, pp. 365-372.
[11] A. Kurganov and D. Levy, Third-order semi-discrete central scheme for conservation laws and convection-diffusion equations, SIAM J. Sci. Comput., 22 (2000), 1461-1488.
[12] A. Kurganov and D. Levy, Central-upwind schemes for the Saint-Venant system, Math. Model. Numer. Anal., 36 (2002), 397-425.
[13] A. Kurganov, S. Noelle and G. Petrova, Semi-discrete central-upwind scheme for hyperbolic conservation laws and Hamilton-Jacobi equations, SIAM J. Sci. Comput., 23 (2001), 707-740.
[14] A. Kurganov and G. Petrova, A third-order semi-discrete genuinely multidimensional central scheme for hyperbolic conservation laws and related problems, Numer. Math., 88 (2001), 683-729.
[15] A. Kurganov and G. Petrova, Central schemes and contact discontinuities, Math. Model. Numer. Anal., 34 (2000), 1259-1275.
[16] A. Kurganov, G. Petrova and B. Popov, Adaptive semi-discrete central-upwind schemes for nonconvex hyperbolic conservation laws, SIAM J. Sci. Comput., submitted.
[17] A. Kurganov and E. Tadmor, New high-resolution central schemes for nonlinear conservation laws and convection-diffusion equations, J. Comput. Phys., 160 (2000), 241-282.
[18] A. Kurganov and E. Tadmor, Solution of two-dimensional Riemann problems for gas dynamics without Riemann problem solvers, Numer. Meth. Part. Diff. Eq., 18 (2002), 584-608.
[19] P. D. Lax, Weak solutions of nonlinear hyperbolic equations and their numerical computation, Commun. Pur. Appl. Math., 7 (1954), 159-193.
[20] B. van Leer, Towards the ultimate conservative difference scheme, V. A second order sequel to Godunov's method, J. Comput. Phys., 32 (1979), 101-136.
[21] R. LeVeque, Finite Volume Methods for Hyperbolic Problems, Cambridge Texts in Applied Mathematics, Cambridge University Press, Cambridge, 2002.
[22] D. Levy, G. Puppo and G. Russo, Central WENO schemes for hyperbolic systems of conservation laws, Math. Model. Numer. Anal., 33 (1999), 547-571.
[23] D. Levy, G. Puppo and G. Russo, Compact central WENO schemes for multidimensional conservation laws, SIAM J. Sci. Comput., 22 (2000), 656-672.

[24] K. A. Lie and S. Noelle, An improved quadrature rule for the flux-computation in staggered central difference schemes in multidimensions, J. Sci. Comput., 63 (2003), 1539-1560.

[25] K. A. Lie and S. Noelle, On the artificial compression method for second-order nonoscillatory central difference schemes for systems of conservation laws, SIAM J. Sci. Comput., 24 (2003), 1157-1174.

[26] X. D. Liu and E. Tadmor, Third order nonoscillatory central scheme for hyperbolic conservation laws, Numer. Math., 79 (1998), 397-425.

[27] R. Liska and B. Wendroff, Comparison of several difference schemes on 1D and 2D test problems for the Euler equations, SIAM J. Sci. Comput., 25 (2004), 995-1017.

[28] H. Nessyahu and E. Tadmor, Non-oscillatory central differencing for hyperbolic conservation laws, J. Comput. Phys., 87 (1990), 408-463.

[29] P. K. Sweby, High resolution schemes using flux limiters for hyperbolic conservation laws, SIAM J. Numer. Anal., 21 (1984), 995-1011.

[30] E. F. Toro, Riemann Solvers and Numerical Methods for Fluid Dynamics: A Practical Introduction, 2nd ed., Springer, Berlin, 1999.

[31] B. Wang and H. Glaz, Second order Godunov-like schemes for gas dynamics with a nonconvex equation of state, AIAA Report AIAA-99-3256, 1999.